ARTICLE

Check for updates

Dynamic urban land extensification is projected to lead to imbalances in the global land-carbon equilibrium

Ryan A. McManamay [1✉], Chris R. Vernon [2], Min Chen[3], Isaac Thompson[2], Zarrar Khan [2] & Kanishka B. Narayan [2]

Human-Earth System Models and Integrated Assessment Models used to explore the land-atmosphere implications of future land-use transitions generally lack dynamic representation of urban lands. Here, we conduct an experiment incorporating dynamic urbanization in a multisector model framework. We integrate projected dynamic non-urban lands from a multisector model with projected dynamic urban lands from 2015 to 2100 at 1-km resolution to examine 1st-order implications to the land system, crop production, and net primary production that can arise from the competition over land resources. By 2100, future urban extensification could displace 0.1 to 1.4 million km^2 of agriculture lands, leading to 22 to 310 Mt of compromised corn, rice, soybean, and wheat production. When considering increased corn production required to meet demands by 2100, urban extensification could cut increases in yields by half. Losses in net primary production from displaced forest, grassland, and croplands ranged from 0.24 to 2.24 Gt C yr^{-1}, potentially increasing land emissions by 1.19 to 6.59 Gt CO_2 yr^{-1}. Although these estimates do not consider adaptive responses, 1st-order experiments can elucidate the individual role of sub-sectors that would otherwise be masked by model complexity.

[1] Department of Environmental Science, Baylor University, Waco, TX 76798, USA. [2] Pacific Northwest National Laboratory, Richland, WA 99354, USA. [3] Department of Forest and Wildlife Ecology, University of Wisconsin Madison, Madison, WI 53706, USA. ✉email: Ryan_McManamay@baylor.edu

Urban expansion and intensified demands for resources have induced global environmental change sufficient to affect the Earth-climate system[1]. Cities have disproportionate effects relative to their spatial footprint—they comprise only 3% of the Earth's terrestrial land surface, yet they house 60% of the world's population and drive 75% of global greenhouse gas emissions[2]. Although localized environmental problems such as heat stress and air pollution are well recognized through the adaptation of global climate models to urban areas[3], the reverse effects of urbanization on regional-to-global land-atmosphere dynamics are still uncertain[4]. Increasing evidence suggests that urban areas can have significant impacts on regional-to-global circulation patterns and carbon budgets through emissions[5] and land-use change via urban extensification[6,7]. By the end of the 21st century, these impacts are only expected to increase as the global urban land total is estimated to grow 100–600%, depending on population growth assumptions[8]. Unfortunately, these estimates may be conservative. New observations suggest the rate of urbanization over the past 30 years is four times higher than previously thought, where urban lands increased 80% relative to a 52% increase in population during the same timeframe[9].

Despite the acknowledged role of the urban built environment on global carbon and climate cycles, the land components of Human–Earth system models (ESMs) and global circulation models (GCMs) lack representation of urban areas[10] or, if included, urban lands are either not dynamic or require hybridization between non-urban land models and urban counterparts[11–16]. The exclusion of urban areas in land models has primarily been a matter of practicality, as they only represent a small portion of the overall land budget, too refined for the granularity of GCM and ESMs. Because most of Earth's land is comprised of natural lands and croplands, ESMs have primarily focused on the land-atmosphere implications of land-use transitions within these major non-urban groups[15,16]. Future projections of land-use and land cover change are typically achieved through Integrated Assessment Models, which derive plausible scenarios for land allocations by accounting for shifting socioeconomic conditions[16,17].

One such example is the Global Change Analysis Model (GCAM), which simulates current and future behaviors and interactions between energy, water, land, climate, and economic systems at regional and global scales[18]. These systems are modeled collectively within a single integrative platform, which operates on the principles of market equilibrium. The land system, in particular, operates based on a profit structure depending on the pursuit of different land uses[19]. Changes in energy and water resources, as well as prices and demands for commodities, will inherently induce changes in land allocations. However, in the current GCAM configuration, urban lands are static, as there is no structure to accommodate urban allocations[17,20].

Multiple studies document the global extent of future impacts of urban land extensification on other socioeconomic sectors and ecosystem services, such as losses in global croplands[21], elevated land emissions due to loss in forest biomass[6], and increased risk to biodiversity hotspots and conservation lands[22]. However, these assessments do not account for dynamic non-urbanized land changes stemming from shifting socioeconomic demands across competing sectors. Growing populations increase the competition over finite land space through simultaneously intensifying demands for urbanization supporting dense settlements, agricultural expansion for sustaining food or biomass production, and reforestation to mitigate carbon emissions. Multisectoral modeling approaches, such as GCAM, balance land areas among competing uses to meet projections in commodities, which are dynamic in space and time (e.g., crop yields, biomass). Not accounting for urban dynamism, however, can upset the land-energy-carbon equilibrium, which has practical implications for model budgeting. More importantly, these imbalances can lead to unforeseen consequences on resources (e.g., crop production[21]), nonlinear and interactive impacts on warming[23], or feedback that offsets potential climate mitigation measures[24].

In recent years, a growing number of urban land modeling efforts have emerged that incorporate socioeconomic drivers and simulate dynamic urban land at high resolutions and at global scales[8,25,26]. Because these models are compatible with other integrated assessment approaches, there are opportunities to reconcile non-urban and urban land modeling systems within multisector and human–Earth system model environments. The intersection of dynamic non-urban lands with dynamic urban lands provides an opportunity to examine the interdependences, interactive stress, and feedback to carbon cycles that can arise from the competition over land resources.

Here, we conduct an analysis that examines how the lack of consideration of one process, urban extensification, may lead to 1st-order imbalances and non-linearities in responses in a human–Earth system model framework. Our work integrates two dynamic, high-resolution, global-scale land modeling systems to examine the intersection of urban and non-urban land extensification and consequences to the equilibrium of other land-dependent commodities and carbon dynamics, depicted in an IAM framework. Specifically, we evaluate the dynamic changes (primarily losses) expected to forested and agricultural systems from urban extensification, and the subsequent effects on global crop yields and terrestrial net primary production, both of which may be temporally dynamic to meet socioeconomic demands (feeding growing populations) or climate mitigation (decarbonization).

Results

In our analysis, urban land projections among Shared Socioeconomic Pathways (SSPs)[27] are governed by the Country-Level Urban Building Scenario (CLUBS) model[8] and downscaled locally by the Spatially Explicit, Long-term, Empirical City development (SELECT) model[28,29]. Urban lands are represented as fractional values (0 to 1) of impervious surface within 1-km grid cells. These were aggregated to 0.05° cells to match the resolution of dynamic non-urban lands. Regional agriculture and forested land-use projections are produced by GCAM, reharmonized to land type definitions from the Community Land Model[15], and downscaled to 0.05° by Demeter, a spatial disaggregation model[30], to produce final non-urban dynamic land products[20]. Non-urban projections vary not only by SSPs but also by land allocations influenced by Representative Concentration Pathways (RCPs), Global Circulation Models (GCMs), and adjustments (harmonization) in the spatial representation of various land classes (Supplementary Table 1).

We integrated dynamic urban lands from the SELECT model with dynamic non-urban lands from GCAM-Demeter model to examine the effects of urban extensification on land cover alterations and subsequent implications to crop yields, net primary production, and carbon emissions. Urban lands are present within the GCAM-Demeter model system but are held static over time. To estimate implications of urban dynamism, urban land change from SELECT, represented as an urban fraction, is compared on a grid-by-grid basis to static urban fraction coverage from GCAM-Demeter to calculate an urban fraction delta (ΔUf) (Fig. 1). ΔUf serves as the basic unit which we estimate losses in non-urban lands and subsequent land-process implications.

In accordance with the modeling results provided in ref. [8], urban lands globally could reach anywhere from 1.2 million under SSP1 to 3.7 million km^2 under SSP5 by 2100 (Fig. 2). This
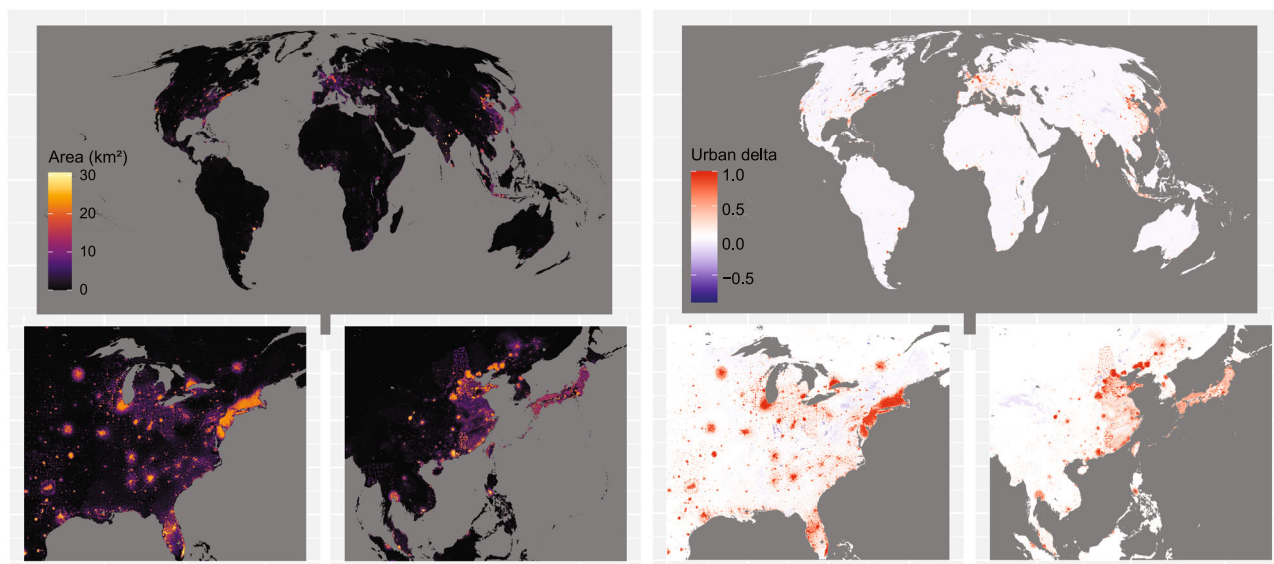
Fig. 1 Urban land projections for 2100 under the Shared Socioeconomic Pathway 5. Urban land per each 0.05° pixel, modeled under CLUBS-SELECT[8], is shown on the left, and the urban land delta, or fractional difference in urban area under SSP5 in 2100 compared to the static urban area depicted by the Global Change Analysis Model and Demeter, is depicted on the right.

represents a 52–380% increase in urban lands from 2015 estimates. By 2100, urbanization appears greatest in the Eastern US and Western US coast, Europe, East Asia, India, and Indonesia (Fig. 1). ΔUf is predominately positive across the world, indicative of increasing urbanization from base values represented in GCAM-Demeter (Fig. 1); however, negative values of ΔUf were apparent in the Northeast, Midwest, Intermountain West of the US, as well as central Asia (Fig. 1). These patterns are indicative of overallocation of urban areas in the Community Land Model (CLM) base map used within the GCAM-Demeter modeling system.

Generally, agricultural lands (crop and pastureland) are most compromised by urban extensification, with up to 1.4 million km^2 lost by the end of the century, an area equivalent to over two times the size of Texas (Table 1 and Fig. 2). Particularly, lands supporting bioenergy crop production predominate these impacted areas, followed by croplands supporting staple products, such as corn, wheat, soybean, and rice (Table 1 and Fig. 2). Losses in forests and grasslands are also substantial, although relative differences in impacts depend on SSP. Grasslands sustained more losses than agricultural lands in SSP1 and more losses than forests in all SSPs, except SSP5 (Table 1). Of forest land classes, temperate forests experience the most losses in total acreage, although tropical forests are observed to decline up to 2% of current levels by 2100 under SSP5 (Table 1 and Fig. 2). Total land budgets are summarized in Supplementary Fig. 1.

Scenarios driving non-urban land areas (from GCAM-Demeter) were numerous ($n = 2700$) and divergent (Supplementary Table 1), which translated into highly variable land area changes arising from urban extensification. Sources of variation explaining global land area changes from urbanization among scenarios were primarily driven by region, followed by year, and SSP (Fig. 3). RCPs had a measurable influence on bioenergy and rainfed cropland alteration, whereas the influence of Global Circulation Models (GCMs) was negligible for all land classes. When considering only the US, the primary drivers of land changes included SSP, year, and source (harmonization between GCAM and CLM base map) (Fig. 3).

Losses in crop yields ranged dramatically across crops, SSPs, and regions (Table 2, Figs. 2 and 4). Losses in corn yield

dominated compromised crop production, followed by losses in rice and wheat (Fig. 4). Highest losses in crop yields are consistently observed in SSP5, followed by SSP2 (Fig. 4). Whereas most losses in yield are globally widespread, compromised rice production is most pronounced in Asia, Africa, and South America (Fig. 4). By 2100, 22–310 Mt (Megatonne or million metric tons) of global annual staple crop production (corn, rice, soybean, and wheat) could be compromised by urban extensification (Table 2); this represents 1–12% of the total 2010 production levels for those staple crops reported by GCAM. By 2050, losses in corn production alone could range from 3 to 85 Mt, and by 2100, these losses could reach 10–219 Mt, constituting anywhere from 2% to 26% of current global corn yields. By 2100, GCAM projections suggest an additional 200–560 Mt per year of corn production is required by 2100 to accommodate increasing populations; hence, urban extensification could counter required increases in yield by 9–43% (Fig. 5). Across all SSPs, projections in corn, rice, and wheat production increase until mid-century and then stabilize or decline. Under SSP5, urban extensification by 2100 could reduce the production of corn and rice below current levels (Fig. 5).

Spatially explicit estimates of net primary production (NPP) rates compromised by urban extensification were generated according to each land cover type and summarized for forest, agriculture, and grasslands (Table 3). Sources of NPP losses generally follow patterns in land classes compromised by urban extensification. Under SSPs 2–4, compromised agriculture lands lead to the highest losses in NPP, followed by grasslands and then forested lands (Fig. 6). Under SSP5, however, NPP losses are noticeably higher in forested lands by 2100. By 2050, total NPP losses range from being negligible up to 0.8 Gt yr^{-1}, which constitutes 1.7% of contemporary global NPP estimates (48–69 Gt)[31]. By the end of the century, NPP losses under SSP5 could exceed 2.3 Gt C yr^{-1} or 3–4% of current NPP levels (Table 3). Losses in NPP associated with compromised agricultural lands were predominately located in the upper midwestern US, east Asia, middle and east Africa, and eastern Europe, whereas NPP lost due to grassland conversion was found in the areas mentioned above in addition to South America (Fig. 6). Forest-associated NPP losses tended to show less regionality, although trends in NPP generally
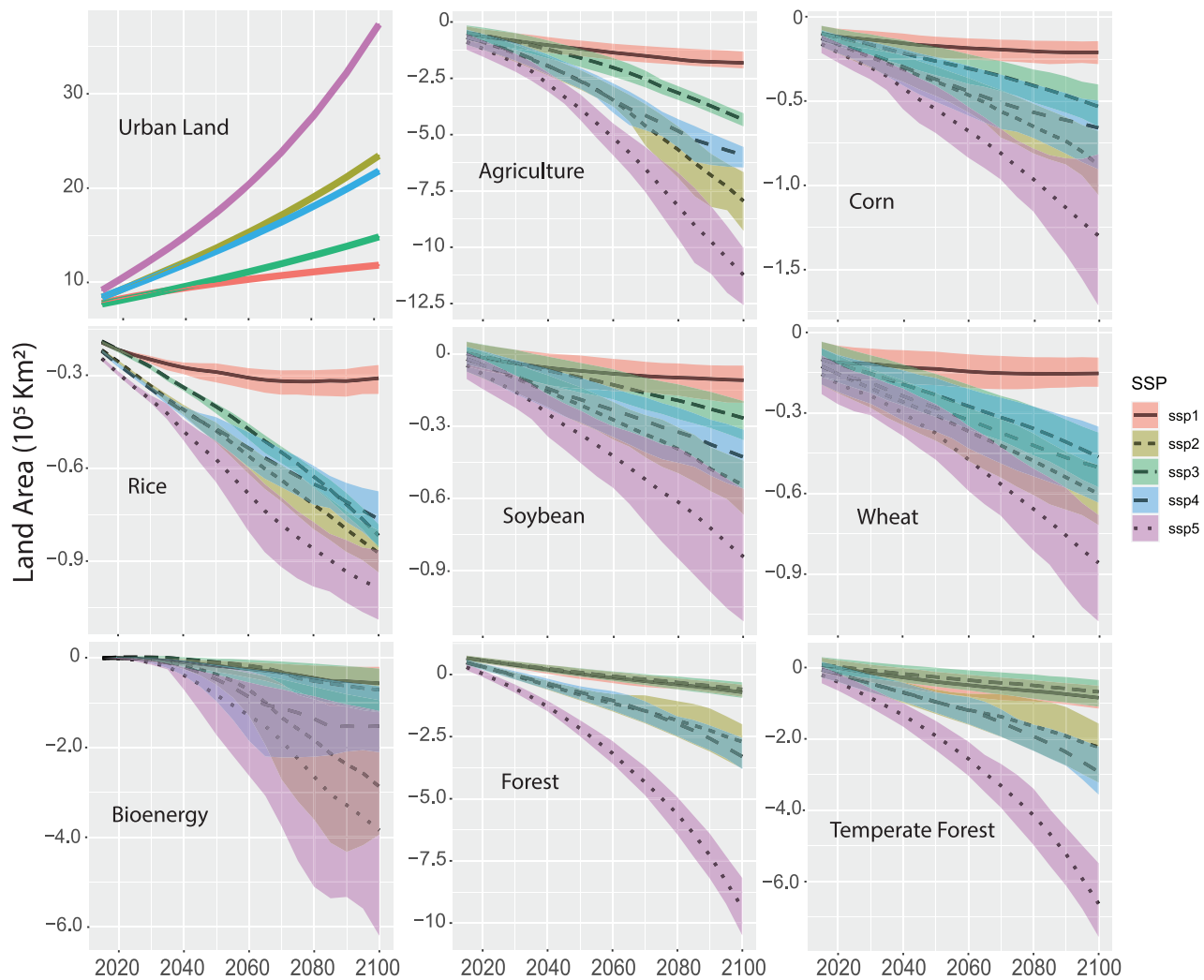
Fig. 2 Global land area adjustments from dynamic urbanization. Urban land changes from the CLUBS-SELECT model (from ref. [8]) according to the Shared Socioeconomic Pathways (SSPs) are displayed on the top left, and resulting land area changes are shown for each land category group. Ranges in values for each SSP represent different scenarios based on Global Circulation Models (GCMs), Representative Concentration Pathways (RCPs), and the land harmonization procedure.

followed similar, but dampened, geographic patterns of agriculture and grasslands (Fig. 6). Based on losses in NPP from urban extensification, annual global-scale land CO_2 emission estimates from GCAM were inflated to account for reduced carbon sequestration (Table 4). Increases in land CO_2 emissions ranged among SSP and RCP combinations (Table 4 and Fig. 7). Estimates ranged from an increase of 1.19 Gt CO_2 yr^{-1}, on average, under SSP1 (from −3.97 to −2.79 Gt yr^{-1}) to an increase of 6.56 Gt CO_2 under SSP5 (from −3.96 to 2.61 Gt yr^{-1}) (Table 4 and Fig. 7).

Discussion

Our results suggest that the exclusion urban land projections within integrated assessment models and by association, Human–Earth System Models, can lead to systemic global imbalances and disequilibria in commodities, such as crop yields, and land-atmospheric interactions. Specifically, we provided evidence that lack of incorporation of urban land dynamism can lead to 1st-order cascading impacts on GCAM's assumptions and outputs for global and regional land and carbon budgets, which ultimately can influence subsequent outcomes by modeling communities and managers. We estimate that by 2100, urban extensification could compromise anywhere from 1 to 12% of

current global production levels for all staple crops combined. The yield loss from individual crops, such as corn, represents almost 50% of the required production increase needed to accommodate growing world populations. We also find that forest and grassland areas comprised by urban expansion are considerable, collectively losing up to 2.2 million km² globally. Likewise, NPP losses due to urban extensification could range from 0.04% to 4.8% of current global annual estimates[31] depending on scenario and uncertainty in NPP values; this could undermine future climate mitigation efforts, leading to potential increases of 1.19–6.56 Gt yr^{-1} in projected CO_2 emissions from the land surface for SSP1 and SSP5, respectively, by 2100. These estimates should be considered conservative since they do not account for secondary or tertiary human adaptations within the Earth system. For instance, croplands displaced by urban extensification would likely be compensated through conversion of grassland and forested systems to agroecosystems[32] or via increased production intensity, which could lead to elevated reductions in NPP and higher CO_2 emissions.

Even without considering the secondary and tertiary responses, these results are surprising since built-up lands, as a portion of Earth's terrestrial land surface, are numerically insignificant. Global estimates of the spatial extent of urban lands by the end of

Table 1 Compromised land areas (losses in land coverage, thousand km²) by 2100 stemming from urban extensification averaged for all scenarios within Shared Socioeconomic Pathways (SSPs).

Land sector	SSP1	SSP2	SSP3	SSP4	SSP5	Min	Max
Agriculture	181	795	434	591	1123	108	1423
Corn	21	88	53	66	130	14	171
Wheat	15	60	46	50	86	9	108
Soybean	11	54	27	43	84	5	111
Cotton	3	15	13	16	18	1	21
Rice	31	87	82	76	99	27	109
Sugar	0	0	0	0	0	0	0
Other crop	45	202	142	188	322	27	384
Bioenergy crop	56	287	71	152	385	20	620
Rainfed crop	116	595	274	422	844	61	1109
Irrigated crop	66	200	160	169	279	47	330
Forest	71	270	59	330	939	31	1049
Temperate forest	84	222	67	292	663	34	756
Boreal forest	−44	−6	−20	−5	45	−53	64
Tropical forest	32	53	12	43	231	6	281
Grasslands	269	509	299	502	787	172	1244

Minima and maxima are also provided across all scenarios, including SSPs, Representative Concentration Pathways (RCPs), Global Circulation Models (GCMs), and for harmonized and non-harmonized land classifications. Negative values indicate increases in land areas.

the century range from 1.5 to 3%, due primarily to inconsistent definitions for "urban land"[33], modeling approaches, or projection products. SELECT utilizes the Global Human Settlement Layer (GHSL)[34], a 38-m empirical Landsat-derived time series dataset for model development and calibration. Urban lands from the SELECT model are synonymous with GHSL as built-up land or impervious surfaces, i.e., manmade materials such cement, asphalt, steel, glass[8]. Projected urbanization via the SELECT model suggests 1.8 to 6-fold increases from levels in 2000 to 2100, ranging from 0.8% of Earth's terrestrial land (1.1 million km²) in SSP1 to 2.5% in SSP5 (3.6 million km²) at the end of the century. Direct comparisons to other studies are made difficult for the reasons stated above. For instance, Chen et al.[26] estimated global urban lands could range from 0.8 to 2 million km² by 2100 under the SSPs, where the upper bounds of urban land area estimates are noticeably lower than those projected by SELECT. The authors similarly utilize GHSL but rely on the Future Land-Use Simulation (FLUS) model[35] to project the probability of occurrence of urban land and, subsequently, binary classifications of urban and non-urban land at 1 km, whereas SELECT produces an urban fraction at the same resolution. In contrast, global projections by Li et al.[25] suggest urban lands could range anywhere from 1.9 to 3.1 million km² under SSP4 and SSP5, respectively, a similar range reported in our study. Multiple studies have suggested tripling of global urban land in only a period of 30 years, suggesting that 6-fold increases by the end of the century may be conservative[6,21]. A 30-year retrospective analysis using high-resolution Landsat satellite data suggested the rate of urbanization is four times higher than previous estimates and becoming increasingly decoupled from population growth[9]. Since the studies listed above all used empirical patterns in urban land changes in relation to population to develop urbanization projection models, this suggests future rates of urbanization are highly uncertain and deserve increasing attention in research development.

Numerous studies have estimated the direct implications of urban extensification on other land sectors and natural resources, particularly cropland loss and deforestation[6,21,26]. A significant difference between our assessment and previous studies is that we examined the intersection and competition between simultaneous dynamic changes in urban land and non-urban lands, both driven by non-stationary competing resource demands. Beyond non-stationarity, the non-urban lands simulated by GCAM were characterized by 2700 different scenarios representing combinations of time, SSPs, RCPs, Global Circulation Models (GCMs), and alternative land-class harmonization procedures (see "Methods"). Hence, our analysis captures considerable uncertainty in the potential outcomes of urbanization on other sectors. Nonetheless, cropland and NPP losses reported in other studies are within the ranges in this study. Urban expansion projections between 2000 and 2030 were estimated to compromise up to 2.4% of global croplands (up to 10% in Asia)[21] and lead to 1.38 Pg of carbon losses in forests, equivalent to 5% of emissions from tropical deforestation and land-use change[6]. Longer-term projections through the end of the century have suggested similar trends. Chen et al.[26] estimate that at least 50% of urban land expansion is expected to compromise croplands, leading to 1–4% declines in annual global crop production. Congruent with other studies, our analysis suggests that croplands are the most impacted based on the spatially explicit nature of urban growth's intersection with dynamic changes in other land sectors. In our study, the location of changes in croplands, accomplished via downscaling by Demeter, is based on land suitability (e.g., low slope and arable soils), in addition to the proximity to pre-existing croplands. Similarly, the location of urban land growth, simulated by SELECT, is higher in areas proximate to existing urbanization and in lands suitable for expansion, primarily flat areas that also tend to be the most conducible for crop production.

Beyond direct impacts on other land systems, urban extensification creates non-linearities in land system responses through land-atmosphere feedbacks. In addition, the indirect or secondary effects of urbanization, such as expansion of displaced croplands or intensification of use on remaining natural lands, have been shown to exceed the direct effects[36]. Hence, lack of accounting for urban dynamics in IAM and ESM frameworks can lead to systemic imbalances in Earth System budgets. Multiple studies report non-linearities between urban-induced losses in forested or cropland area and land-dependent processes. For instance, Chen et al.[26] report 1% losses in global croplands due to urbanization projected through the end-of-century, which led to disproportionate losses (up to 4%) in crop yield. In a retrospective global analysis from 2000 to 2010, newly urbanized areas comprised only 0.04% of Earth's land surface yet constituted 9% of global carbon emissions from fossil fuels and cement[24]. Likewise, we observed 1–12% losses in corn cropland area from 2010 estimates, whereas losses in corn yield were disproportionately higher (1–26%). This suggests that urban extensification is likely to displace the most productive croplands, as also found by Bren d'Amour et al.[21]. Furthermore, our study suggests urban extensification could result in up to 4% losses in NPP yet lead to increases in GCAM carbon emissions sufficient to alter the land-atmosphere interface from that of net carbon sequestration to net emissions before 2100. Apart from direct impacts from extensification, urbanization can also induce cascading and multiplicative indirect impacts on Earth's land system through teleconnections[37]. Indirect effects of urbanization, such as urban-induced cropland displacement on losses in natural land, can be greater than 10-fold larger than the direct effects of urban land displacement[32,36].

Climate-induced shifts in terrestrial carbon sequestration are highly uncertain[38–41]; hence, the added role of land conversion
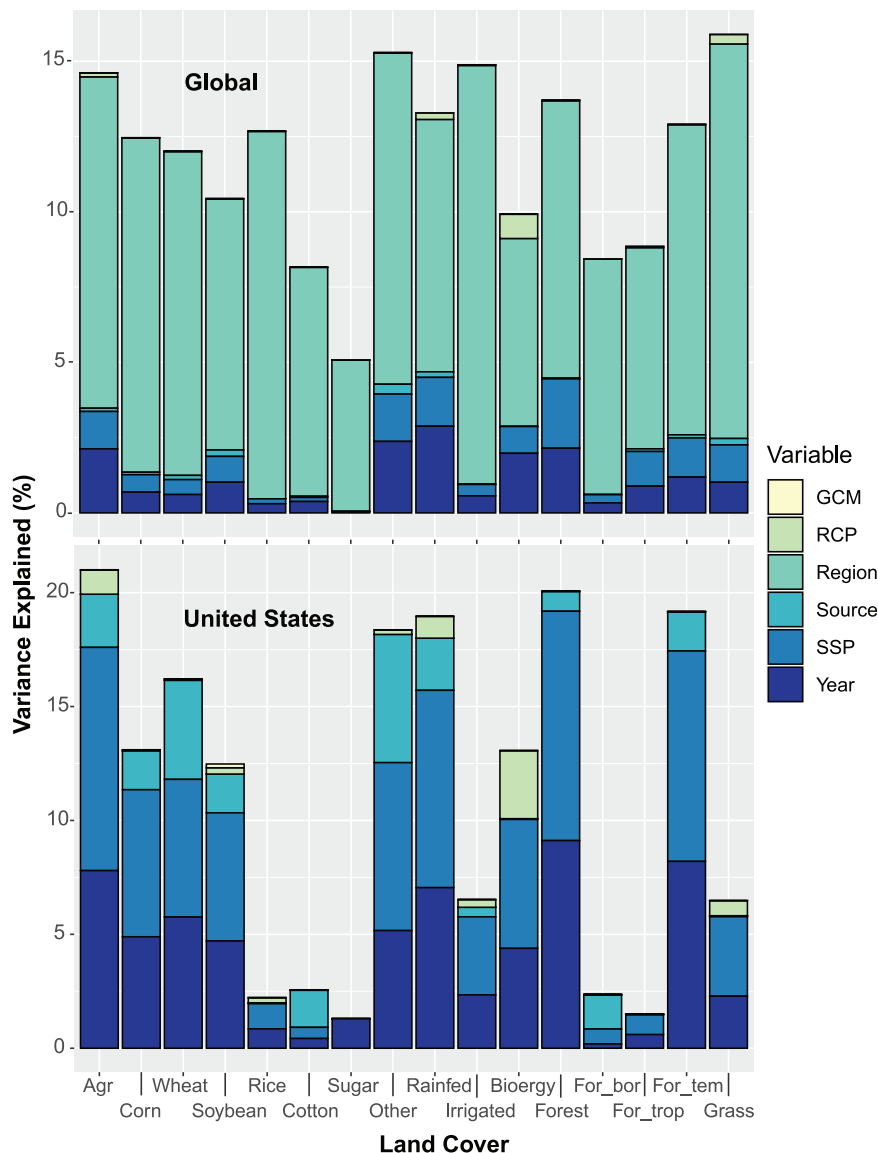
Fig. 3 Sources of variation in land area losses to urbanization. Linear models of land area (km^2) lost to urbanization were constructed for the entire globe and only the United States (US) using variables responsible for divergent scenarios and included the Global Circulation Model (GCM), Representative Concentration Pathway (RCP), global regions (global model only), source (land harmonization), Shared Socioeconomic Pathways (SSPs), and year. The percent variation explained was calculated using an Analysis of Variance.

and shifts in land-atmospheric dynamics only adds more complexity and uncertainty. For instance, rapid urbanization between 2000 and 2010 offset climate-driven increases in NPP during the same timeframe (primarily from warming temperatures) by 30%[24]. Most urbanization is projected to occur in the northern hemisphere, with notable losses to temperate forests. Rates of NPP in the northern hemisphere could increase under warming via extended growing seasons and elevated CO$_2$ conditions[42], creating negative feedbacks on atmospheric carbon levels and hence, dampening the potential impacts of urban extensification. However, in cases where Earth's terrestrial system is saturated by atmospheric CO$_2$ levels or experience seasonal temperature shifts, these ecosystems could release more CO$_2$ or even become net sources[39,43]. In addition, urban areas dissipate sufficient heat to alter continental scale warming pattern, an additional positive forcing[5]. In these cases, urban extensification could expedite the timeline for hitting these thresholds through increasing the rate of removal of terrestrial carbon sinks. Another important consideration is the response from not only forested ecosystems, but

also agroecosystems. Our results reveal that NPP losses from urban extensification are substantial due to deforestation in addition to cropland loss. Although agriculture extensification and deforestation has led to declines in global NPP, agricultural NPP rates (1.8 kg C m^{-2} yr^{-1}) are only slightly lower than forest values (2.0 kg C m^{-2} yr^{-1})[44].

Our analysis has several limitations that could be addressed in future work. Urban land projections in our study are derived from only one model (CLUBS-SELECT), although several new studies report global high-resolution projections through end-of-century[25,26,45]. When placed within the context of Earth's terrestrial land surface, differences in global urban land projections are relatively small. By 2100, the upper boundary of urban land expansion from SELECT comprises only 2.43% of Earth's terrestrial land, relative to a maximum of 1.35% reported in Chen et al.[26]. Even so, these small differences could result in nonlinear responses to other sectors, as our results suggest. We elected to use SELECT because of its ability to capture mechanistic urbanization processes—future urban land projections are, in part, an

outcome of past urban trajectories and urban maturity where urbanization rates are temporally dynamic and locally dependent, with parameters that can be adjusted in tune with SSPs—a major difference from other urban land model approaches[8,28]. We perceive SELECT as providing more realism, but also an important capability to accommodate more flexibility and thematic consistency with the assumptions underlying the SSPs. However, CLUBS-SELECT does not consider competition between urbanization and other land types. Indeed, our analysis assumes urbanization will expand into suitable areas, as needed, to accommodate population growth, since urban land is prioritized over other land uses. Aside from localized cases, we presume urbanization at global scales will inevitably outcompete other land uses because the price or value of urban land far exceeds other land types[46]. Only until the global land value system changes, or non-urban lands become scarce, will societies value non-urban uses sufficiently to dampen urbanization.

As another limitation, our experiment only examines 1st-order implications of urban dynamism and does not account for secondary or tertiary human adaptations, such as compensatory cropland expansion and increasing pressure on existing natural resource areas (e.g., wood harvest), both of which could be directly incorporated into GCAM's equilibrium modeling framework. Crop production losses are estimated based on localized, yet static yield estimates that are not responsive to climate. In addition, GCAM does not accommodate endogenous climate influences on crop yields and by association, cropland requirements, as could be captured in a crop model. Even so, crop production responses to climate change are highly uncertain, where long-term precipitation and temperature shifts could induce modest global yield increases[47], yet extreme climate events could lead to dramatic reductions in yield[48]. Finally, we only consider CO_2 emissions related to loss of above-ground carbon sequestration potential and not CO_2 emitted from mechanical disturbances, such as clearing forest and grassland, or disruption to soil ecosystems. Ultimately, this would suggest our altered NPP and CO_2 emissions are conservative estimates.

Ultimately, urban land extensification is expected to increase stress on finite resources required for socioeconomic transitions. Among the largest impacts to the agricultural sectors were losses in bioenergy croplands (50,000–400,000 km^2) to support energy transitions in the transportation (biofuels) and electricity (biomass combustion) sectors. Under GCAM's projections for both SSP1 and SSP5, biomass crops increase from being virtually non-existent in 2015 to a global estimate of 3 million km^2 to 7 million km^2 by 2100, depending on the emission scenario. This suggests urban extensification could compromise 1% to 13% of global lands

Table 2 Losses in crop yields (million metric tons) stemming from urban extensification averaged for scenarios within Shared Socioeconomic Pathways (SSPs) for 2050 and 2100.

Crop	SSP1	SSP2	SSP3	SSP4	SSP5	Min	Max
2050							
Cotton	0.21	0.55	0.38	0.63	0.76	0.04	1.01
Corn	11.4	35.7	18.1	35.5	63.4	2.94	85.0
Rice	10.6	17.5	15.5	17.3	21.0	9.19	24.3
Soybean	1.02	2.97	1.52	2.73	4.62	0.25	6.03
Sugar	0.07	0.09	0.07	0.11	0.09	0.03	0.16
Wheat	3.53	8.53	6.44	7.71	10.4	2.01	13.1
2100							
Cotton	0.26	1.64	1.52	1.58	1.83	0.12	2.24
Corn	17.1	93.0	43.6	67.6	165	9.96	219
Rice	11.4	31.4	31.3	27.0	36.5	9.20	41.1
Soybean	1.43	7.11	3.54	5.47	11.11	0.71	14.9
Sugar	0.02	0.08	0.03	0.10	0.03	0.00	0.16
Wheat	3.88	16.6	12.8	13.3	23.6	2.44	30.8

Minima and maxima are also provided across all scenarios, including SSPs, Representative Concentration Pathways (RCPs), Global Circulation Models (GCMs), and harmonized and non-harmonized land classifications.
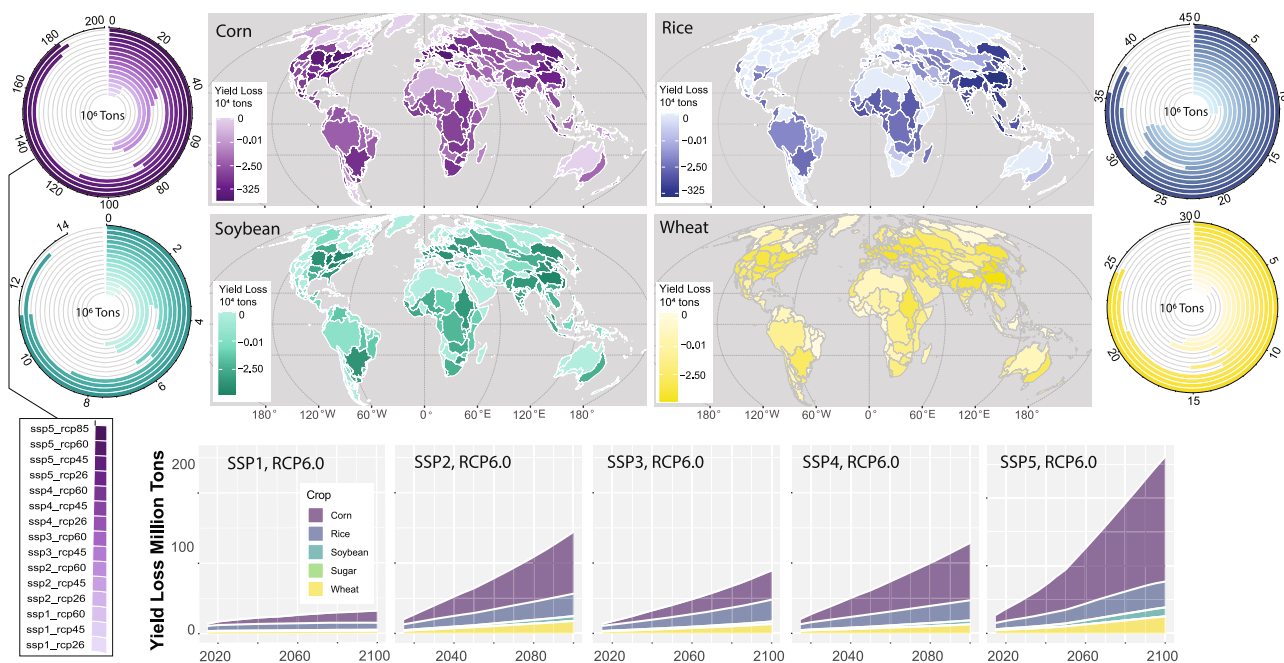

Fig. 4 Losses in crop yields due to land conversion from urban extensification. Global maps display crop yield losses (metric tons yr^{-1}) for the scenario, including harmonized land cover for Shared Socioeconomic Pathway (SSP) 5, Representative Concentration Pathway (RCP 6.0), and the Geophysical Fluid Dynamics Laboratory's Global Circulation Model (GCM) for year 2100. Circular bar plots display losses in crop yields across all SSP-RCP combinations as averages across harmonized and unharmonized land cover and GCMs. Staked area plots represent losses in crop yields, averaged for GCMs and harmonization, for all SSPs for RCP 6.0.
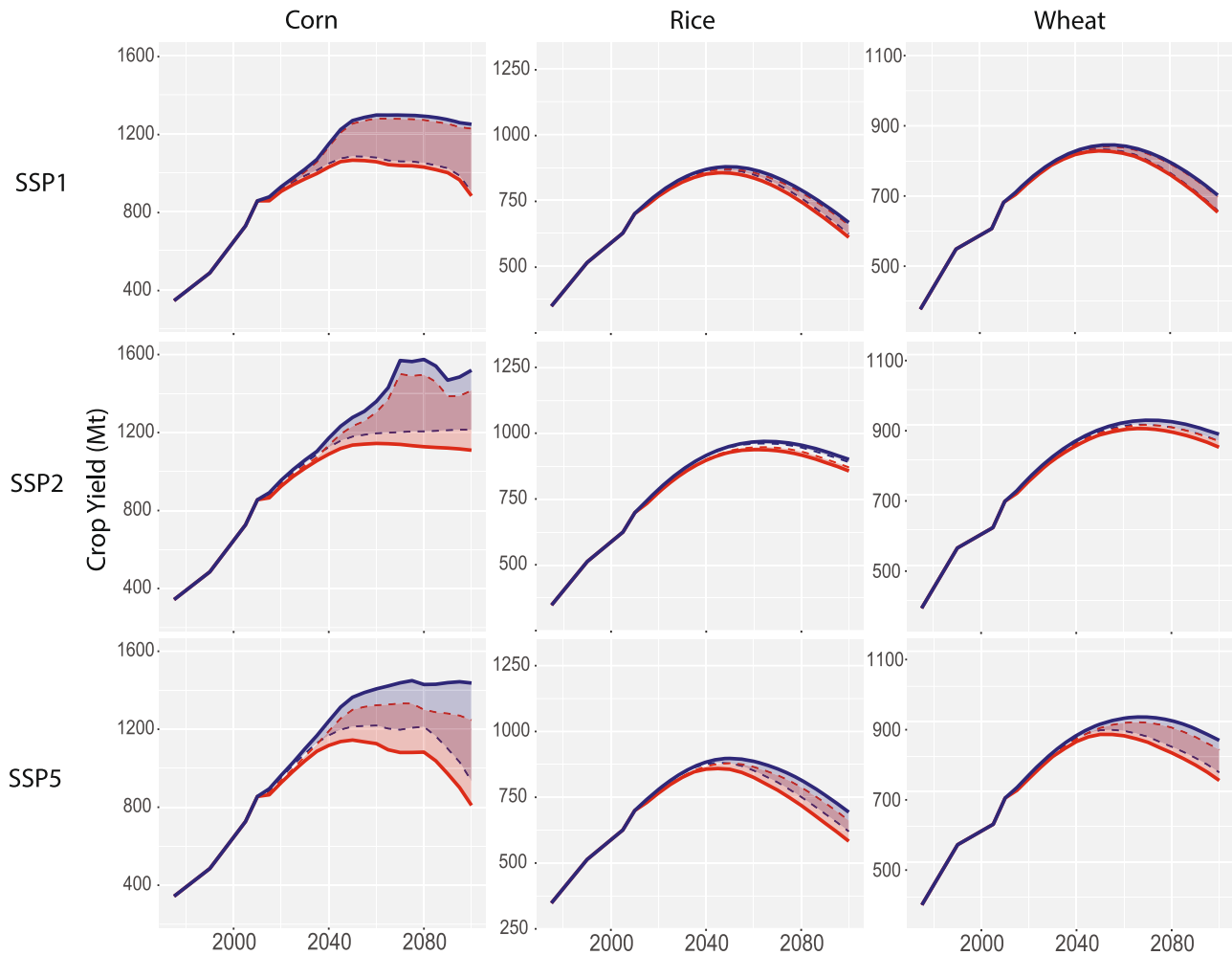
Fig. 5 Reductions in projected staple crop yields due to urban-induced losses in croplands. GCAM crop yield projections (blue areas) were adjusted to account for losses in yield from urban extensification (red areas). Ranges in yields represent variations according to Representative Concentration Pathways (RCPs), Global Circulation Models (GCMs), and for harmonized and non-harmonized land classifications.

dedicated to bioenergy production. By doing so, urban land extensification could counteract climate mitigation and adaptation strategies. For instance, under RCP 2.6 emission scenarios under SSP1 and SSP5, reforestation efforts lead to net carbon sequestration (Fig. 7); however, elevated CO_2 emissions from urban extensification could switch land-atmospheric budgets from net sequestration to net emissions. In other cases, urban extensification can exacerbate shifting land cover, such as decreasing forested lands due to growing croplands in SSP3 RCP 6.0, and growing bioenergy lands under RCP 4.5 in SSP2 and SSP3.

Without even considering competing land-use demands for urban-induced losses, rates of global crop harvests for direct food consumption are unlikely to meet growing food security demands, even by 2030[49]. Addressing these land disequilibria within multisector IAM frameworks, such as GCAM, can be relatively straightforward by reoptimizing balances among competing demands. Within GCAM, loss in croplands and yields will result in increased price[19]; however, staple crops are price inelastic and hence, GCAM will allocate demand through increased production efficiency or increasing cropland area elsewhere (as staple crops are a requirement for global food subsidies), leading to increased natural land displacement, perhaps less suitable for crop production. Increased production efficiencies or fostering crop production in less-productive lands are

both likely to require increased irrigation and fertilizer inputs, placing additional strain on finite resources.

The real-world implication of land budget imbalances is that difficult decisions will continue regarding land service tradeoffs, many of which are mutually exclusive[50]. Direct and indirect urban-induced pressures on agricultural, forest, and grassland ecosystems will continue, leading to increased stress on an overcommitted system. Wise and highly efficient use of land systems, such as consolidation of agricultural lands and increased production efficiency[51], are required to meet these challenges. Adaptations are also needed for the governance of urban land development to preserve productive croplands[26] and natural land integrity[36]. Heterogeneity in global lateral expansion of built-up lands and per-capita urban land area has been shown to be largely dependent on economic structure more so than population growth[52], suggesting that containment strategies (i.e., growth boundaries) that mitigate against market-led development are required to facilitate vertical growth[53]. Unfortunately, urban growth boundaries, without enforcement and regional coordination, have shown to be ineffective at enhancing densification or infilling and preventing sub-urban sprawl[54,55]. Blending market-based, containment, and zoning policies, as well as regional coordination to preserve surrounding crop and natural lands, has been suggested as an effective approach to govern urban growth[55].

Table 3 Losses in net primary production (NPP, gigatons Carbon yr⁻¹) stemming from urban extensification averaged for scenarios within Shared Socioeconomic Pathways (SSPs) for 2050 and 2100.

	SSP1	SSP2	SSP3	SSP4	SSP5	Min	Max
2050							
Agriculture low	0.049	0.108	0.064	0.111	0.163	0.031	0.229
Agriculture medium	0.064	0.139	0.083	0.142	0.208	−0.009	0.290
Agriculture high	0.079	0.170	0.102	0.174	0.253	0.082	0.352
Forest low	0.004	0.051	−0.003	0.046	0.138	0.110	0.151
Forest medium	0.004	0.065	−0.005	0.059	0.179	0.140	0.194
Forest high	0.004	0.080	−0.007	0.071	0.220	-0.012	0.238
Grassland low	0.099	0.145	0.101	0.134	0.176	-0.015	0.214
Grassland medium	0.135	0.199	0.138	0.184	0.242	0.042	0.299
Grassland high	0.171	0.253	0.175	0.234	0.308	0.193	0.384
Total low	0.151	0.304	0.162	0.291	0.477	0.245	0.489
Total medium	0.203	0.403	0.216	0.385	0.628	0.137	0.637
Total high	0.254	0.502	0.270	0.479	0.780	0.054	0.787
2100							
Agriculture low	0.076	0.329	0.170	0.251	0.488	0.045	0.625
Agriculture medium	0.099	0.431	0.222	0.325	0.621	0.025	0.795
Agriculture high	0.123	0.534	0.275	0.400	0.754	0.076	0.965
Forest low	0.048	0.165	0.038	0.200	0.578	0.102	0.650
Forest medium	0.062	0.214	0.048	0.256	0.752	0.224	0.845
Forest high	0.077	0.264	0.058	0.312	0.927	0.032	1.040
Grassland low	0.112	0.210	0.126	0.206	0.310	0.039	0.484
Grassland medium	0.155	0.291	0.176	0.285	0.435	0.061	0.682
Grassland high	0.197	0.372	0.225	0.364	0.560	0.306	0.880
Total low	0.236	0.704	0.333	0.657	1.376	0.388	1.401
Total medium	0.316	0.937	0.445	0.866	1.808	0.128	1.855
Total high	0.397	1.170	0.558	1.077	2.241	0.077	2.310

Minima and maxima are also provided across all scenarios, including SSPs, Representative Concentration Pathways (RCPs), Global Circulation Models (GCMs), and harmonized and non-harmonized land classifications. Low, medium, and high refer to variable per-unit-area coefficients of NPP according to land classes within regions and basins. Negative values indicate increases in NPP.

Methods

Future land projection datasets. Global land-use simulations at 0.05° resolution for 2015–2100 under 15 plausible combinations of Shared Socioeconomic Pathways (SSPs) and Representative Concentration Pathways (RCPs) were obtained from ref. [20]. Future societal and environmental conditions were simulated within the Global Change Analysis Model (GCAM v5.0) to produce land-use allocations for 231 countries (termed regions) and 235 basins for the world under different SSP, RCP, and Global Circulation Model (GCM) combinations. Chen et al.[20] then used a spatial disaggregation model, Demeter[30,56], to downscale coarse land-use projections from GCAM to a local 0.05° × 0.05° grid at 5-yr timesteps. Demeter requires a base map as 'seed' locations to allocate projected land-use area to target grid cells[56]. Although Demeter is flexible in that it can use any base map, one issue is that the selected base map land classes may vary from those characterized in GCAM. In particular, Chen et al.[20] used the base map from the Community Land Model 5 (CLM5) in the Community Earth System Model 2 (CESM), which includes 79 plant functional types (PFTs). These 79 PFTs are analogous yet vary from GCAM's 39 land classes. Chen et al. defined 32 land classes as a final hybrid land classification that preserved the maximum fidelity of class types while reconciling differences among land models. Even so, there are inconsistent differences between land type classifications between the base map and GCAM (e.g., grassland and barren lands) that require reconciliation. To accomplish this, Chen et al. devised a harmonization procedure to adjust the area of GCAM land classes to match the base map classes while maintaining the fractional land-use changes as projected by GCAM in future timesteps. Downscaled results were developed using both the harmonization procedure and unadjusted GCAM land allocations. In total, 2700 LULCC simulations were produced as a combination of 15 SSP-RCP combinations, 5 GCMs, 18 timesteps (2015–2100), and for both the harmonized and unharmonized land classes (Supplementary Table 1).

Although non-urban land types are dynamic and influenced by shifting socioeconomic pressures within the GCAM environment, urban lands within GCAM are static and held constant from the base year (2005) to 2100. To intersect dynamic urban landscapes with GCAM-Demeter-derived land cover, we used simulated urban fraction lands from the Spatially Explicit, Long-term, Empirical City development (SELECT) model[8,28,29]. SELECT is a spatial model that provides decadal changes in urban land fraction at a 1/8° resolution but is constrained by the Country-Level Urban Building Scenario (CLUBS) model, which captures macroscale socioeconomic patterns and varies according to a country's current urbanization trajectory and maturity[8]. The rationale employed within CLUBS is very analogous to the GCAM equilibrium environment, and hence was a thematically consistent product to use for integrating dynamic urban land with dynamic non-urban land changes. Gao and O'Neill[8] developed 1/8° simulations for all five SSPs from 2000 to 2100, and subsequently, these products were downscaled to a 1-km resolution[29]. We used the 1-km downscaled projections to intersect with the Demeter-produced land products.

Integrating GCAM-Demeter with SELECT. Our entire workflow is provided in Supplementary Fig. 2. Because of the difference in spatial resolution, we aggregated the 1-km SELECT product to a 0.05° resolution and projected the rasters to match the coordinate system of Chen et al.[20]. We then interpolated 5-yr timesteps between decadal timesteps of SELECT to match the temporal resolution of Demeter simulations. Both the SELECT and Demeter products represent land cover as fractions, s and d, respectively. However, d is represented as a whole number

Table 4 Land CO$_2$ emissions (Gt CO$_2$ yr^{-1}) for 2050 and 2100 according to various combinations of Shared Socioeconomic Pathways (SSPs) and Representative Concentration Pathways (RCPs) and based on static versus dynamic urban land changes.

SSP	RCP	Static urban		Dynamic urban		Difference
		Mean	Range	Mean	Range	
2050						
ssp1	rcp26	−11.1	(−11.2, −10.8)	−10.3	(−10.6, −9.90)	0.79
	rcp45	−3.47	(−3.53, −3.37)	−2.70	(−2.95, −2.41)	0.77
	rcp60	−0.71	(−0.99, −0.48)	0.05	(−0.41, 0.463)	0.77
ssp2	rcp26	6.83	(6.33, 7.23)	8.32	(7.466, 9.065)	1.49
	rcp45	1.93	(1.58, 2.36)	3.42	(2.721, 4.198)	1.49
	rcp60	1.16	(0.82, 1.42)	2.65	(1.955, 3.258)	1.49
ssp3	rcp45	5.48	(5.01, 5.93)	6.29	(5.635, 6.940)	0.81
	rcp60	3.16	(2.82, 3.48)	3.98	(3.439, 4.489)	0.82
ssp4	rcp26	4.66	(4.12, 5.02)	6.09	(5.214, 6.785)	1.43
	rcp45	−0.92	(−1.26, −0.56)	0.50	(−0.17, 1.191)	1.42
	rcp60	1.15	(0.88, 1.34)	2.58	(1.964, 3.095)	1.42
ssp5	rcp26	−11.1	(−11.3, −10.9)	−8.8	(−9.51, −8.04)	2.33
	rcp45	−10.2	(−10.2, −9.98)	−7.8	(−8.49, −7.13)	2.32
	rcp60	−5.16	(−5.42, −4.95)	−2.85	(−3.65, −2.11)	2.31
	rcp85	−0.33	(−0.56, −0.04)	1.96	(1.183, 2.779)	2.29
2100						
ssp1	26	−4.28	(−4.34, −4.13)	−3.07	(−3.42, −2.63)	1.21
	45	−6.31	(−6.51, −5.70)	−5.12	(−5.61, −4.23)	1.19
	60	−1.33	(−1.46, −1.22)	−0.17	(−0.58, 0.238)	1.16
ssp2	26	−4.96	(−5.13, −4.75)	−1.58	(−2.58, −0.54)	3.38
	45	26.0	(21.3, 27.5)	29.3	(23.8, 31.7)	3.38
	60	−0.37	(−0.50, −0.27)	3.07	(2.11, 3.99)	3.43
ssp3	45	2.68	(2.55, 2.90)	4.31	(3.79, 4.93)	1.63
	60	3.51	(3.16, 4.04)	5.14	(4.40, 6.08)	1.64
ssp4	26	−5.89	(−6.08, −0.63)	−2.69	(-3.62, −1.68)	3.20
	45	0.68	(0.23, 1.05)	3.80	(2.62, 4.90)	3.12
	60	−0.28	(−0.54, −0.06)	2.86	(1.85, 3.82)	3.14
ssp5	26	−8.05	(−8.12, −7.96)	−1.39	(−3.01, 0.237)	6.67
	45	−1.92	(−2.22, −1.75)	4.63	(2.80, 6.32)	6.56
	60	−4.72	(−4.94, −4.43)	1.88	(0.12, 3.70)	6.59
	85	−1.13	(−1.31, −0.90)	5.31	(3.61, 7.05)	6.44

Static urban refers to naïve or default estimates from the Global Change Analysis Model, whereas dynamic urban accounts for projected changes in urban land from SELECT and subsequent losses in net primary production (NPP). Difference refers to dynamic urban mean – static urban mean. Ranges represent variation in non-urban lands due to Global Circulation Models (GCMs), and for harmonized and non-harmonized land classifications, as well as variable estimates of NPP.

percentage (integer). The change in urban fraction, or urban fraction delta (ΔUf), for each grid cell, i, for each of the 2700 scenarios was calculated as:

$$\Delta Uf_i = s_i - \frac{d_i}{100} \qquad (1)$$

Note that ΔUf_i can be negative in cases where the either SELECT or the CLM5 base map has either over-allocated urban lands or has inaccuracies in the spatial depiction of urban lands. The remaining cumulative fraction of all non-urban lands for the ith grid cell is denoted by R where:

$$T_i = 100 - d_i \qquad (2)$$

One universally consistent assumption is that urban land expansion compromises all other non-urban lands. Hence, fractions for the kth non-urban Demeter land type (LF) can be adjusted, denoted as $\overline{LF}$, to accommodate urban land expansion or contraction as follows:

$$\overline{LF_{ki}} = \frac{LF_{ki}}{100} - \left(\frac{LF_{ki}}{T_i} \times \Delta Uf_i \right) \qquad (3)$$

The non-urban land area (LA) compromised or expanded for each land type through urban land expansion or contraction,

respectively, can then be calculated for each grid cell as:

$$\Delta LA_{ki} = \frac{LF_{ki}}{T_i} \times \Delta Uf_i \times A_i \times -1 \qquad (4)$$

Where A is the total area (km^2) of the ith grid cell. Values are multiplied by −1 to indicate losses and gains in non-urban land areas as negative and positive values, respectively. We grouped ΔLA_{ki} into 13 functional land types within three major categories: forest, grassland, and agriculture (including bioenergy). For each of the 2700 scenarios, ΔLA_{ki} and grouped ΔLA_{ki} values were summarized across the regions and basins, and their unique combinations, depicted by the Moirai land system used within GCAM[57].

To understand the sources of variability driving differences in ΔLA_{ki} across scenarios, we constructed linear models for global results where ΔLA_{ki} within basins were a function of region, SSP, RCP, GCM, year, and source, an indicator of harmonized or unharmonized land allocation ($n = 517,007$ observations). To examine within-region variability, we constructed linear models only for the US to explore the importance of all other variables besides region. Analysis of Variance (ANOVA) was used to explore sources of variation explained by each variable.

Effects of dynamic urbanization on crop yields. Following our calculation of land areas compromised by urban extensification,
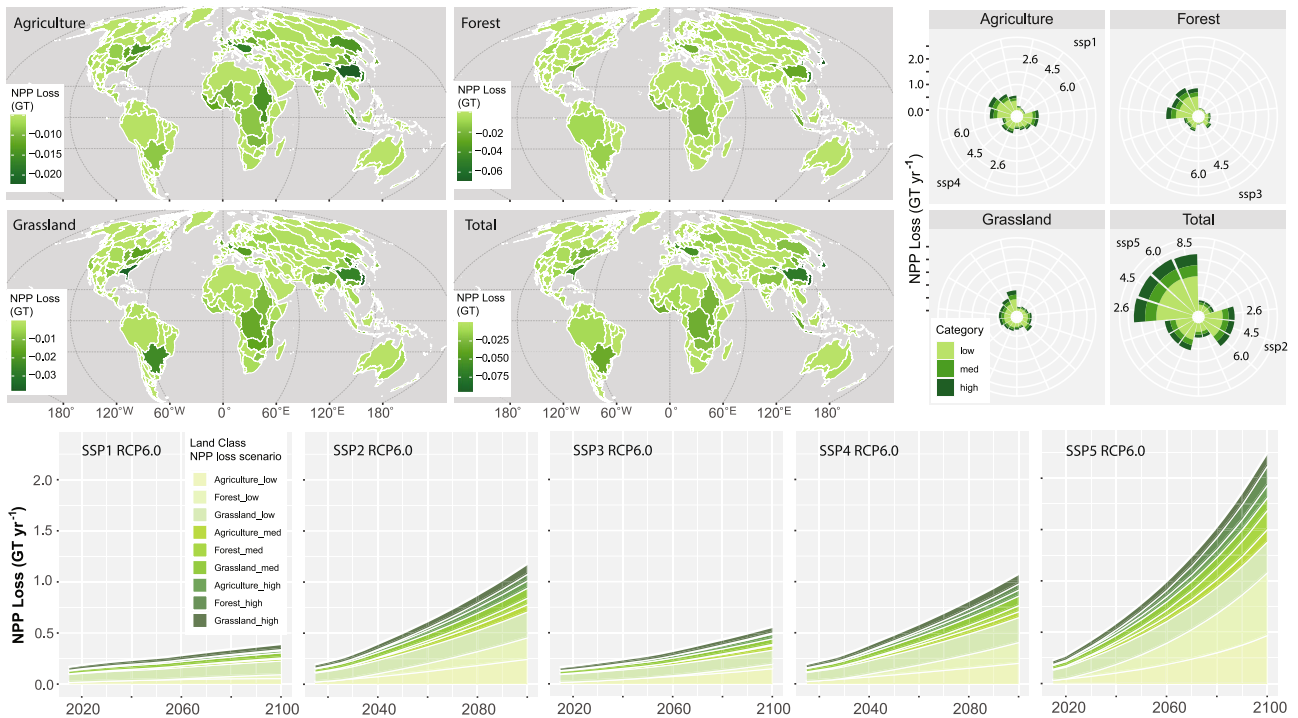
Fig. 6 Losses in net primary production (NPP) from urban extensification. Global maps display average NPP losses (gigatons (GT) Carbon yr^{-1}) for the corresponding displaced land categories from urban extensification for the scenario, including harmonized land cover for Shared Socioeconomic Pathway (SSP) 5, Representative Concentration Pathway (RCP 6.0), and the Geophysical Fluid Dynamics Laboratory's Global Circulation Model for the year 2100. Radial stacked bar plots display losses in NPP (for variable NPP rates), averaged over harmonized and unharmonized land cover and GCMs, for each SSP and RCP combination. Staked area plots represent variable NPP rates for each land category, averaged for GCMs and harmonization, for RCP 6.0 for all SSPs.

we then explored the implications of these changes on global crop yields and net primary production. Global crop yields (tons per hectare) at a 5-min (~10-km) resolution were obtained from ref. [58] and were summarized within the GCAM Moirai region-basin combinations to produce region- and basin-specific averages of crop yields ($\bar{y}$) for corn, cotton, wheat, rice, soybean, sugar crops, and wheat, as these crops align with the cropland types in the final 32-land-class GCAM-Demeter simulations. ΔLA values for each scenario were grouped by compatible functional types (k) and summed for region (r) and basin (b) combinations. Total lost or gained yield (ΔY) for the kth land class was calculated for the rth region and bth basin combination, as:

$$\Delta Y_{krb} = \Delta LA_{krb} \times \bar{y}_{krb} \qquad (5)$$

Where $\bar{y}$ is the average crop yield rate from ref. [58] for the specific crop type (k), region (r), and basin (b) combination.

Effects of dynamic urbanization on net primary productivity. Annual MODIS net primary productivity (NPP), measured in g C m^{-2} y^{-1} in 500-m gridded datasets, were obtained from 2010 to 2015[59]. Annual values were averaged into 5-yr values and then aggregated to 0.05° grid cells to match the GCAM-Demeter resolution. NPP is expected to be non-stationary in the future yet highly uncertain[38,39]. Climate projections suggest increases in NPP in boreal forests of the Northern Hemisphere through the end-of-century[42]; however, the role of climate in NPP trends in the Southern Hemisphere even for recent years (2000–2020) is largely unresolved[24,40,41,60]. Due to this uncertainty, we use a range of estimates to estimate NPP losses. Because LF_{ki} values were fractionated for each 0.05° grid cell and because NPP values were per-unit-area averages, we could not arbitrarily assign NPP

values to individual land classes, even on a proportional basis, within a grid cell. Instead, we created a data frame of unique LF_{ki} values and NPP values for each grid cell observation. For each of the k land types, the data frame was filtered to only consider LF_{ki} grid values $\geq 10\%$, and then those subsets of NPP values were summarized as minima, maxima, and averages within each region-basin as indicative of the range of primary production for a given land class in that area. This can otherwise be stated as:

$$\forall i, k, r, b \mid LF_{kirb} \geq 0.1 \rightarrow NPP_{kirb} \qquad (6)$$

and

$$\min\left(NPP_{krb}\right) = \min_{i} \left\{NPP_i\right\}_{i=1}^{n} \qquad (7)$$

$$\max\left(NPP_{krb}\right) = \max_{i} \left\{NPP_i\right\}_{i=1}^{n} \qquad (8)$$

$$\overline{NPP_{krb}} = \frac{\sum_{i=1}^{n} NPP_i}{n}, \qquad (9)$$

where n is the number of grid cells corresponding to the kth land-class type in each region (r) and basin (b) combination. NPP values were converted from g C m^{-2} y^{-1} to Gt C km^{-2} y^{-r}. Total NPP losses or gains (ΔNPP) associated with urban land changes were calculated as:

$$\min(\Delta NPP_{krb}) = \Delta LA_{krb} \times \min\left(NPP_{krb}\right) \qquad (10)$$

$$\max(\Delta NPP_{krb}) = \Delta LA_{krb} \times \max\left(NPP_{krb}\right) \qquad (11)$$

$$\overline{\Delta NPP_{krb}} = \Delta LA_{krb} \times \overline{NPP_{krb}} \qquad (12)$$
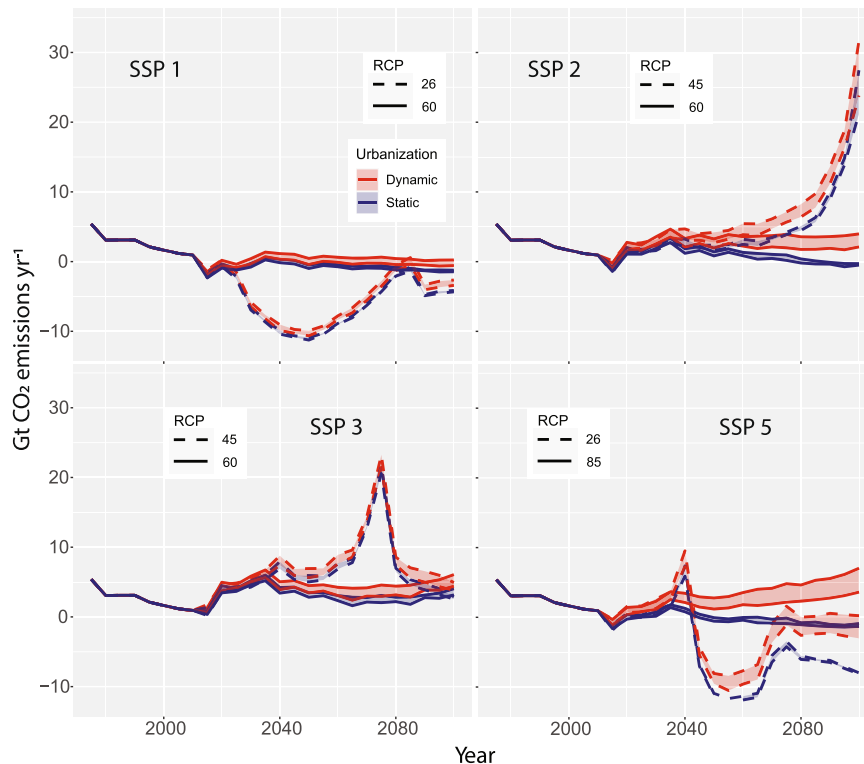
Fig. 7 Implications of urban-induced land alterations on global CO² emissions. Urbanization-induced losses in net primary production and impacts to global CO_2 emission projections were summarized across Shared Socioeconomic Pathway (SSP) and Representative Concentration Pathways (RCP). Projections in CO_2 from the Global Change Analysis Model (GCAM) (blue lines) were adjusted to account for losses in carbon sequestration due to land conversion from urban extensification (red areas). Ranges in values represent variations according to Global Circulation Models (GCMs) and for harmonized and non-harmonized land classifications.

First-order implications of urban dynamism on GCAM land-carbon equilibria. Because GCAM is an equilibrium model, shifting socioeconomic demands, such as increasing population growth, and natural resources, such as crops and land, as well as emissions and atmospheric concentrations of greenhouse gases, are interrelated and balanced. We evaluated the implications of compromised land cover, reduced crop yields, and losses in NPP due to urban extensification on GCAM's budgetary allocations for agricultural commodities and carbon emissions from land-use change. All outputs in our study utilize GCAM v5.0. Relevant simulated outputs from GCAM include annual crop yields (Mt yr^{-1}) and annual carbon dioxide (CO_2) emissions (Mt Carbon yr^{-1}) for various sectors, including those from land-use change provided at 5-yr increments (1975–2100) under SSPs, RCPs, and GCM combinations. Hence, our estimates of changes in crop yields and NPP from urban extensification can be placed into the context of Earth system components simulated from GCAM. In GCAM, land-use change CO_2 emissions are calculated using a simple accounting approach[61], where emissions from above-ground vegetation and soils are due to changes in carbon stock (ΔC) from land use and dependent upon regionally explicit carbon densities[62]. Emissions calculated from ΔC reflect the immediate year for vegetation, whereas soil emissions have a prolonged lag effect specified for each region[62]. Here, we assume that ΔNPP is strictly associated with compromised above-ground forest, grassland, or cropland vegetation, and that $\Delta NPP < 0$ directly increases CO_2 emissions from the land surface. We also assume that NPP estimates for urban land are 0.

Changes in crop yield (ΔY_{krb}) stemming from urban extensification were added or negated from GCAM simulated estimates of crop yield for all scenarios and years. Cumulative land-use-related CO_2 emissions from GCAM were adjusted to account for reduced sequestration of CO_2 based on changes in NPP (ΔNPP) arising from urban extensification. We accomplished this by first converting GCAM land CO_2 from Mt C to Gt C. CO_2 emissions and ΔNPP estimates were them converted from C to CO_2 equivalent by multiplying by 3.664 ($CO_2 = 44.01$ g mol^{-1}; C = 12.011 g mol^{-1}). CO_2 equivalent values from ΔNPP were then added to GCAM's estimates of CO_2 emissions stemming from land-use change.

Data availability

Code availability

References
1. Seto, K. C. & Satterthwaite, D. Interactions between urbanization and global environmental change. *Curr. Opin. Environ. Sustain.* **2**, 127–128 (2010).
2. Grimm, N. B. et al. Global change and the ecology of cities. *Science* **319**, 756–760 (2008).
3. Zheng, Z., Zhao, L. & Oleson, K. W. Large model structural uncertainty in global projections of urban heat waves. *Nat. Commun.* **12**, 3736 (2021).

4. Qian, Y. et al. Urbanization impact on regional climate and extreme weather: current understanding, uncertainties, and future research directions. *Adv. Atmos. Sci.* **39**, 819–860 (2022).

5. Zhang, G., Cai, M. & Hu, A. Energy consumption and the unexplained winter warming over northern Asia and North America. *Nat. Clim. Change* **3**, 466–470 (2013).

6. Seto, K. C., Güneralp, B. & Hutyra, L. R. Global forecasts of urban expansion to 2030 and direct impacts on biodiversity and carbon pools. *Proc. Natl. Acad. Sci. USA* **109**, 16083–16088 (2012).

7. Churkina, G. The role of urbanization in the global carbon cycle. *Front. Ecol. Evol.* **3**, 144 (2016).

8. Gao, J. & O'Neill, B. C. Mapping global urban land for the 21st century with data-driven simulations and Shared Socioeconomic Pathways. *Nat. Commun.* **11**, 2302 (2020).

9. Liu, X. et al. High-spatiotemporal-resolution mapping of global urban change from 1985 to 2015. *Nat. Sustain.* **3**, 564–570 (2020).

10. Zhao, L. et al. Global multi-model projections of local urban climates. *Nat. Clim. Chang.* **11**, 152–157 (2021).

11. Grimmond, C. S. B. et al. The international urban energy balance models comparison project: first results from phase 1. *J. Appl. Meteorol. Climatol.* **49**, 1268–1292 (2010).

12. Grimmond, C. S. B. et al. Initial results from Phase 2 of the international urban energy balance model comparison. *Int. J. Climatol.* **31**, 244–272 (2011).

13. Li, D., Malyshev, S. & Shevliakova, E. Exploring historical and future urban climate in the Earth System Modeling framework: 1. Model development and evaluation. *J. Adv. Model. Earth Syst.* **8**, 917–935 (2016).

14. Li, D., Malyshev, S. & Shevliakova, E. Exploring historical and future urban climate in the Earth System Modeling framework: 2. impact of urban land use over the continental United States. *J. Adv. Model. Earth Syst.* **8**, 936–953 (2016).

15. Lawrence, D. M. et al. The community land model version 5: description of new features, benchmarking, and impact of forcing uncertainty. *J. Adv. Model. Earth Syst.* **11**, 4245–4287 (2019).

16. Hurtt, G. C. et al. Harmonization of global land use change and management for the period 850–2100 (LUH2) for CMIP6. *Geoscientific Model. Development* **13**, 5425–5464 (2020).

17. Riahi, K. et al. The Shared Socioeconomic Pathways and their energy, land use, and greenhouse gas emissions implications: an overview. *Glob. Environ. Chang.* **42**, 153–168 (2017).

18. Calvin, K. et al. GCAM v5. 1: representing the linkages between energy, water, land, climate, and economic systems. *Geosci. Model Dev.* **12**, 677–698 (2019).

19. Wise, M., Calvin, K., Kyle, P., Luckow, P. & Edmonds, J. A. E. Economic and physical modeling of land use in GCAM 3.0 and an application to agricultural productivity, land, and terrestrial carbon. *Clim. Change Econ.* **5**, 1450003 (2014).

20. Chen, M. et al. Global land use for 2015–2100 at 0.05 resolution under diverse socioeconomic and climate scenarios. *Sci. Data* **7**, 320 (2020).

21. Bren d'Amour, C. et al. Future urban land expansion and implications for global croplands. *Proc. Natl. Acad. Sci. USA* **114**, 8939–8944 (2017).

22. McDonald, R. I., Kareiva, P. & Forman, R. T. The implications of current and future urbanization for global protected areas and biodiversity conservation. *Biol. Conserv.* **141**, 1695–1703 (2008).

23. Krayenhoff, E. S. et al. Diurnal interaction between urban expansion, climate change and adaptation in US cities. *Nat. Clim. Change* **8**, 1097–1103 (2018).

24. Liu, X. et al. Global urban expansion offsets climate-driven increases in terrestrial net primary productivity. *Nat. Commun.* **10**, 5558 (2019).

25. Li, X. et al. Global urban growth between 1870 and 2100 from integrated high resolution mapped data and urban dynamic modeling. *Commun. Earth Environ.* **2**, 201 (2021).

26. Chen, G. et al. Global projections of future urban land expansion under Shared Socioeconomic Pathways. *Nat. Commun.* **11**, 537 (2020a).

27. O'Neill, B. C. et al. A new scenario framework for climate change research: the concept of Shared Socioeconomic Pathways. *Clim. Change* **122**, 387–400 (2014).

28. Gao, J. O'Neill. Data-driven spatial modeling of global long-term urban land development: The SELECT model. *Environ. Model. Softw.* **119**, 458–471 (2019).

29. Gao, J. & Pesaresi, M. Downscaling SSP-consistent global spatial urban land projections from 1/8-degree to 1-km resolution 2000-2100. *Sci. Data.* **8**, 281 (2021).

30. Vernon, C. R. et al. Demeter–a land use and land cover change disaggregation model. *J. Open Res. Softw.* **6**, PNNL-SA–131044 (2018).

31. Gough, C. M. Terrestrial primary production: fuel for life. *Nat. Educ. Knowl.* **3**, 28 (2011).

32. van Vliet, J. Direct and indirect loss of natural area from urban expansion. *Nat Sustain* **2**, 755–763 (2019).

33. Liu, Z. et al. How much of the world's land has been urbanized, really? A hierarchical framework for avoiding confusion. *Landscape Ecol.* **29**, 763–771 (2014).

34. European Commission. *GHSL—Global Human Settlement Layer*. https://ghsl.jrc.ec.europa.eu/. (2023)

35. Liu, X. et al. A future land use simulation model (FLUS) for simulating multiple land use scenarios by coupling human and natural effects. *Landsc. Urban Plan.* **168**, 94–116 (2017).

36. Ren, Q., He, C., Huang, Q., Shi, P., Zhang, D. & Güneralp, B. Impacts of urban expansion on natural habitats in global drylands. *Nat. Sustain.* **5**, 869–878 (2022).

37. Seto, K. C. et al. Urban land teleconnections and sustainability. *Proc. Natl. Acad. Sci. USA* **109**, 7687–7692 (2012).

38. Friedlingstein, P. et al. Climate–carbon cycle feedback analysis: results from the C4MIP model intercomparison. *J. Clim.* **19**, 3337–3353 (2006).

39. Heimann, M. & Reichstein, M. Terrestrial ecosystem carbon dynamics and climate feedbacks. *Nature* **451**, 289–292 (2008).

40. Zhao, M. & Running, S. W. Drought-induced reduction in global terrestrial net primary production from 2000 through 2009. *Science* **329**, 940–943 (2010).

41. Potter, C., Klooster, S. & Genovese, V. Net primary production of terrestrial ecosystems from 2000 to 2009. *Clim. Change* **115**, 365–378 (2012).

42. Beltrán-Sanz, N. et al. Climate change leads to higher NPP at the end of the century in the Antarctic Tundra: response patterns through the lens of lichens. *Sci. Total Environ.* **835**, 155495 (2022).

43. Tang, R. et al. Increasing terrestrial ecosystem carbon release in response to autumn cooling and warming. *Nat. Clim. Chang.* **12**, 380–385 (2022).

44. Krause, A. et al. Quantifying the impacts of land cover change on gross primary productivity globally. *Sci. Rep.* **12**, 18398 (2022).

45. Zhou, Y., Varquez, A. C. & Kanda, M. High-resolution global urban growth projection based on multiple applications of the SLEUTH urban growth model. *Sci. Data* **6**, 34 (2019).

46. Albouy, D., Ehrlich, G. & Shin, M. Metropolitan land values. *Rev. Econ. Stat.* **100**, 454–466 (2018).

47. Lobell, D. B. & Gourdji, S. M. The influence of climate change on global crop productivity. *Plant Physiol.* **160**, 1686–1697 (2012).

48. Moriondo, M., Giannakopoulos, C. & Bindi, M. Climate change impact assessment: the role of climate extremes in crop yield simulation. *Clim. Change* **104**, 679–701 (2011).

49. Ray, D. K. et al. Crop harvests for direct food use insufficient to meet the UN's food security goal. *Nat. Food* **3**, 367–374 (2022).

50. Gerecke, M. et al. Assessing potential landscape service trade-offs driven by urbanization in Switzerland. *Palgrave Commun.* **5**, 109 (2019).

51. Duan, J. et al. Consolidation of agricultural land can contribute to agricultural sustainability in China. *Nat. Food* **2**, 1014–1022 (2021).

52. Sun, L., Chen, J., Qinglan, L. & Huang, D. Dramatic uneven urbanization of large cities throughout the world in recent decades. *Nat. Commun.* **11**, 5366 (2020).

53. Zhao, P. Managing urban growth in a transforming China: evidence from Beijing. *Land Use Policy* **28**, 96–109 (2011).

54. Jun, M.-J. The effects of Portland's urban growth boundary on urban development patterns and commuting. *Urban Stud.* **41**, 1333–1348 (2004).

55. Fertner, C. et al. Urban sprawl and growth management—drivers, impacts and responses in selected European and US cities. *Fut. Cit. Env.* **2**, 9 (2016).

56. Chen, M., Vernon, C. R., Huang, M., Calvin, K. V. & Kraucunas, I. P. Calibration and analysis of the uncertainty in downscaling global land use and land cover projections from GCAM using Demeter (v1. 0.0). *Geosci. Model Dev.* **12**, 1753–1764 (2019).

57. Di Vittorio, A. V., Vernon, C. R. & Shu, S., Moirai version 3: a data processing system to generate recent historical land inputs for global modeling applications at various scales. *J. Open Res. Softw.* **8**, 1 (2020).

58. Monfreda, C., Ramankutty, N. & Foley, J. A. Farming the planet: 2. Geographic distribution of crop areas, yields, physiological types, and net primary production in the year 2000, Global Biogeochem. *Cycles* **22**, GB1022 (2008).

59. Running, S., Mu, Q. & Zhao, M. MOD17A3H MODIS/Terra Net Primary Production Yearly L4 Global 500m SIN Grid V006 [data set]. *NASA EOSDIS Land Processes DAAC*. Accessed 2022-12-13. https://doi.org/10.5067/MODIS/MOD17A3H.006 (2015).

60. Heinrich, V. H. et al. Large carbon sink potential of secondary forests in the Brazilian Amazon to mitigate climate change. *Nat. Commun.* **12**, 1785 (2021).

61. Houghton, R. A. The annual net flux of carbon to the atmosphere from changes in land use 1850-1990. *Tellus* **51B**, 298–313 (1999).

62. JGCRI (Joint Global Change Research Institute). *GCAM v7 Documentation: The GCAM Land Allocation Module*. https://jgcri.github.io/gcam-doc/land.html (2023).

63. Gao, J. "Global 1-km Downscaled Urban Land Fraction Grids, SSP-Consistent Projections and Base Year, v1 (2000 - 2100)". *Harvard Dataverse, V1* https://doi.org/10.7910/DVN/0EGDOK (2021).

64. Chen, M. et al. Global land use for 2015-2100 at 0.05° resolution under diverse socioeconomic and climate scenarios. *Pacific Northwest National Laboratory 2; PNNL* https://doi.org/10.25584/data.2020-07.1357/1644253 (2020).

Acknowledgements

Author contributions

R.A.M. conceived the paper, conducted the analysis and code development, and drafted the manuscript. C.R.V. assisted with high-performance computation, code development, and editing. M.C. contributed to the initial integration of SELECT and Demeter products. I.T. and Z.K. contributed GCAM crop yield and emission outputs and edited the manuscript. K.B.N. provided content on systemic implications of GCAM disequilibria and edited the manuscript.

Competing interests

The authors declare no competing interests.

Additional information

Supplementary information The online version contains supplementary material available at https://doi.org/10.1038/s43247-024-01231-y.

Correspondence and requests for materials should be addressed to Ryan A. McManamay.

Peer review information *Communications Earth & Environment* thanks the anonymous reviewers for their contribution to the peer review of this work. Primary Handling Editors: Jinfeng Chang and Martina Grecequet. A peer review file is available.

Reprints and permission information is available at http://www.nature.com/reprints

Publisher's note Springer Nature remains neutral with regard to jurisdictional claims in published maps and institutional affiliations.